Chan, C.-H., Stein, R. (2009): Stress evolution following the 1999 Chi-Chi, Taiwan, earthquake: Consequences for afterslip, relaxation, aftershocks, and departures from Omori decay. - Geophysical Journal International, 177, 1, 179-192

DOI: 10.1111/j.1365-246X.2008.04069.x

Geophys. J. Int. (2009) **177**, 179–192 doi: 10.1111/j.1365-246X.2008.04069.x

Stress evolution following the 1999 Chi-Chi, Taiwan, earthquake: consequences for afterslip, relaxation, aftershocks and departures from Omori decay

Chung-Han Chan[1*] and Ross S. Stein[2]

[1]*GFZ German Research Centre for Geosciences, Section of Seismic Hazard and Stress Field, Potsdam, Germany. E-mail: han@gfz-potsdam.de*
[2]*U. S. Geological Survey, Menlo Park, California, USA*

Accepted 2008 December 8. Received 2008 November 14; in original form 2008 March 5

SUMMARY

We explore how Coulomb stress transfer and viscoelastic relaxation control afterslip and aftershocks in a continental thrust fault system. The 1999 September 21 M_w = 7.6 Chi-Chi shock is typical of continental ramp-décollement systems throughout the world, and so inferences drawn from this uniquely well-recorded event may be widely applicable. First, we find that the spatial and depth distribution of aftershocks and their focal mechanisms are consistent with the calculated Coulomb stress changes imparted by the coseismic rupture. Some 61 per cent of the $M > 2$ aftershocks and 83 per cent of the $M > 4$ aftershocks lie in regions for which the Coulomb stress increased by >0.1 bars, and there is a 11-12 per cent gain in the percentage of aftershocks nodal planes on which the shear stress increased over the pre-Chi Chi control period. Second, we find that afterslip occurred where the calculated coseismic stress increased on the fault ramp and décollement, subject to the condition that friction is high on the ramp and low on the décollement. Third, viscoelastic relaxation is evident from the fit of the post-seismic GPS data on the footwall. Fourth, we find that the rate of seismicity began to increase during the post-seismic period in an annulus extending east of the main rupture. The spatial extent of the seismicity annulus resembles the calculated ≥0.05-bar Coulomb stress increase caused by viscoelastic relaxation and afterslip, and we find a 9–12 per cent gain in the percentage of focal mechanisms with >0.01-bar shear stress increases imparted by the post-seismic afterslip and relaxation in comparison to the control period. Thus, we argue that post-seismic stress changes can for the first time be shown to alter the production of aftershocks, as judged by their rate, spatial distribution, and focal mechanisms.

Key words: Time series analysis; Earthquake interaction, forecasting and prediction; Seismicity and tectonics.

1 INTRODUCTION

Many studies have examined the hypothesis that static stress changes influence the spatial or temporal distribution of aftershocks and subsequent large shocks (see reviews by Harris 1998; Stein 1999; King & Cocco 2000; Freed 2005; Steacy *et al.* 2005). However, only few such studies have analysed large thrust earthquakes (Parsons 2002; Lin & Stein 2004; Ma *et al.* 2005), and fewer still benefit from the rich seismic catalogue (Chang *et al.* 2000), and dense GPS (Yu *et al.* 2001) and accelerometer (Ma *et al.* 2001) networks in Taiwan.

Ma *et al.* (2005) argued that the Chi-Chi event exhibits unequivocal evidence of Coulomb stress transfer in promoting aftershocks, with increases and decreases in the $M > 2$ seismicity rate corresponding to calculated Coulomb stress change, although the seismicity rate decreases in the Coulomb stress shadows do not become evident until 2–3 months after the main shock. The Chi-Chi main shock was calculated to promote failure on the rupture planes of most $M > 4$ aftershocks, and nearly all of the ten $M > 6$ aftershocks that struck within the first year were found to be promoted by several bars by the coseismic stresses. In addition, for large events such as Chi-Chi, afterslip, lower crust-upper mantle viscoelastic rebound and large aftershocks themselves may cause measurable post-seismic deformation (Rundle & Jackson 1977; Thatcher 1983; Savage 1990), which we study here. The seven continuous and 80 campaign GPS stations of Taiwan also provide an unprecedented opportunity to study the post-seismic deformation following the Chi-Chi earthquake.

Here we investigate the role of the coseismic stresses in promoting the afterslip, and we test whether stresses imparted by the afterslip and viscoelastic rebound modified the distribution and decay of aftershocks. Although many studies have proposed such a mechanism (Pollitz *et al.* 2004; Freed 2005;

* Formerly at: Institute of Geophysics, National Central University, Chung-Li, Taiwan.

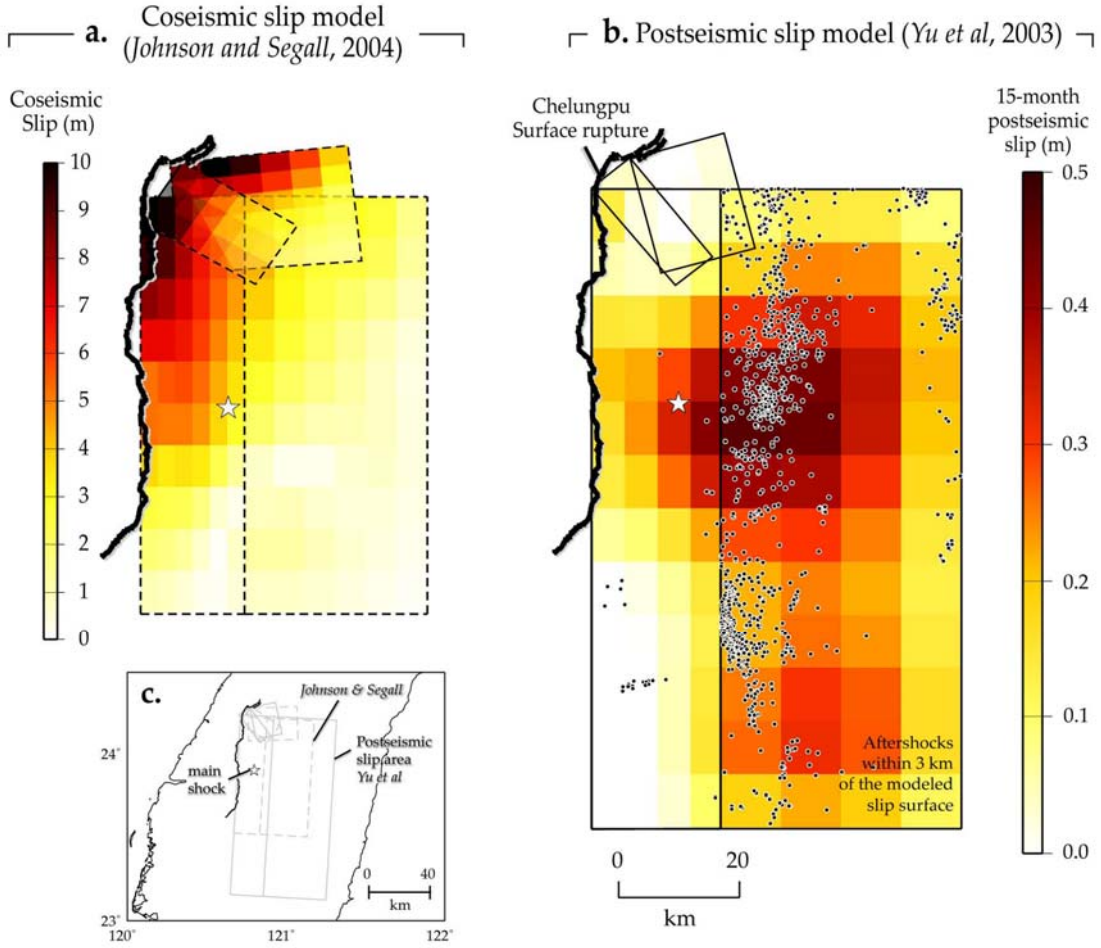

Figure 1. Coseismic slip distribution from (a) Johnson & Segall (2004) from geodetic data, with a thrust ramp and a horizontal décollement at depth of 7.7 km; the smaller rectangles are the northern segments (b) The 15-month afterslip distribution from Yu *et al.* (2003), with a ramp segment dipping 26° and a horizontal décollement at 10.4 km. The first 3 months of aftershocks occurring within 3 km of the rupture planes are shown as black dots. (c) Map-view of the model fault geometries; dashed rectangles correspond to the coseismic model; solid rectangles to the post-seismic model.

Freed *et al.* 2007), none has demonstrated a change in the aftershock migration, distribution or rate corresponding to relaxation or afterslip.

2 MODELS AND METHODS

2.1 Coseismic and post-seismic slip models derived from GPS observations

We calculate the Coulomb stress changes for Chi-Chi coseismic slip models obtained by Johnson & Segall (2004) (Fig. 1a). The several studies that have illuminated the kinematics of the Chi-Chi rupture process (e.g. Ma *et al.* 1999, 2001; Chi *et al.* 2001; Zeng & Chen 2001; Ji *et al.* 2003; Johnson & Segall 2004; Perfettini & Avouac 2004) contain consistent features, such as large coseismic displacements in the northern portion of the Chelungpu fault. Johnson & Segall (2004) employ a four-plane fault geometry with a subhorizontal décollement located at ' 8 km depth to explain the significant GPS deformation observed in central Taiwan (Fig. 2a). Due to the paucity of GPS stations southeast of the epicentre, the quality of the model becomes questionable over the southeastern part of the décollement. These models undoubtedly over-simplify the structure of the Chelungpu thrust system, which is highly corrugated and might also contain slip on a shallower décollement in the Chinshui shole as well as slip on a deep portion of the sub-vertical Shuilikeng fault, as advocated by Yue *et al.* (2005). We nevertheless adopt the simpler geometry used by those modelling the geodetic and microearthquake data, so that the inverted coseismic and postseismic slip are consistent with the source geometry.

We use the afterslip model of Yu *et al.* (2003), which attributes the first 15 months of observed GPS displacements exclusively to afterslip (Figs 1b and 2b). Slip is resolved on four planes with a subhorizontal décollement located at -10 km depth, covering a much larger area than the coseismic model (Fig. 1c). Yu *et al.* (2003) placed the décollement at 10 km depth, whereas Johnson and Segall (2004) placed it at 8 km; this adds a small complication to our analysis, but the 2 km difference is not resolvable from the geodetic and seismic data. Yu *et al.* find two slip asperities, downdip from the main

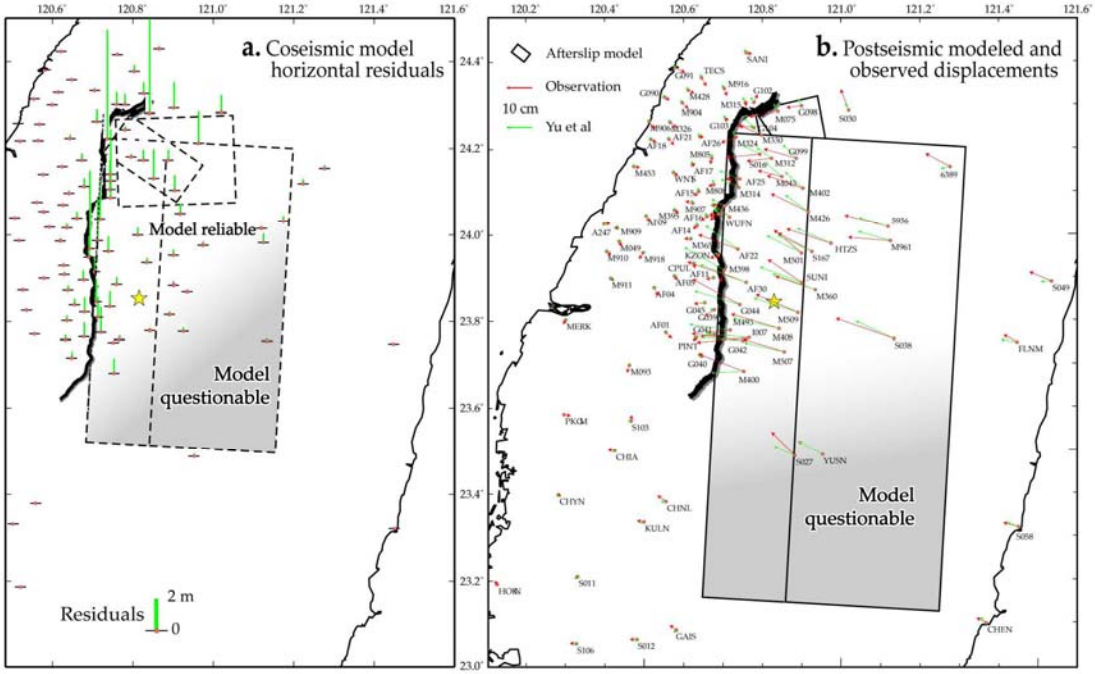

Figure 2. (a) Horizontal GPS displacement residuals for the two coseismic models. (b) Observed and modelled displacements during first 15-month post-seismic period after the Chi-Chi earthquake. Note lack of coverage in the southern part of the décollement.

shock hypocentre and another to the south of the coseismic slip. By contrast, to the north where the maximum coseismic displacement occurred, the inferred afterslip is relatively modest.

The Yu *et al.* model fits the GPS data on the hanging wall quite well, but systematically misfits the footwall observations (Fig. 2b). Because the hanging wall displacements are generally about four times larger than those on the footwall, models that minimize the combined rms residuals need not satisfy the footwall deformation despite the large number of footwall GPS stations. Only two GPS stations (S027 and YUSN in Fig. 2b) constrain the location, size and slip in the southern asperity of Yu *et al.* Since displacements of ^-10 cm at these stations are significant, slip to the south of the coseismic rupture is required, but its location and the slip minima between the northern and southern patches poorly determined.

2.2 Viscoelastic deformation model

We employ VISCO1D (Pollitz *et al.* 2006) in a spherical layered earth with the viscosity structure (Fig. 3c). Based on interseismic GPS data, Johnson *et al.* (2005) inferred a high asthenospheric viscosity (2.0 x 1019 Pa s) throughout Taiwan except perhaps beneath Central Range, where the viscosity could be lower (Sheu & Shieh 2004; Hsu 2004). With the assumed structure we explore the contribution of viscoelastic deformation to the observed GPS displacements and Coulomb stress changes. The surface displacements from viscoelastic deformation greatly reduces the GPS residuals in the footwall 10–25 km from the Chelungpu fault (blue shaded area in Fig. 3a). Over the décollement and in the hanging wall, however, the observed displacements are dominated by afterslip (Fig. 2b), and the calculated viscoelastic deformation is modest (Fig. 3b). Thus, while viscoelastic deformation is more subtle than afterslip, both processes are likely active.

Neither the afterslip model of Yu *et al.* (2003) nor viscoelastic deformation satisfies the observed GPS displacements within 5– 10 km of the Chelungpu fault on the footwall block (yellow shaded area in Fig. 3a). A possible explanation for this misfit could be about 15 cm of post-seismic slip on the Changhua fault elucidated by Yue *et al.* (2005) (blue line in Fig. 3a).

2.3 Methods

We calculate the Coulomb failure stress (ACFS) resolved onto specified fault planes inferred from focal mechanisms of M > 4 aftershocks, in which $\Delta CFS = \Delta\tau + \mu'\Delta\sigma$, where $\Delta\tau$ is the shear stress change, μ' is effective friction coefficient, and $\Delta\sigma$ is the unclamping (or normal) stress change (King *et al.* 1994; Toda *et al.* 1998). Generally μ' is modelled in most studies to lie between 0.4 and 0.8. However, there is evidence that highly lubricated faults or those with large cumulative slip such as the central San Andreas fault may have $\mu' < 0.2$ (Zoback *et al.* 1987; Toda & Stein 2002), whereas jagged, anastomosing faults with rough or cohesive surfaces and little cumulative slip can have $\mu' < 0.8$ (Parsons *et al.* 1999; Lin & Stein 2004). We also tested the assumption of constant friction against the isotropic poroelastic assumption in computing Coulomb stress changes (Beeler *et al.* 2000; Cocco & Rice 2002), but for reasonable values of dry friction (0.75) and Skempton's coefficients (0.5–0.9), the results were indistinguishable from each other.

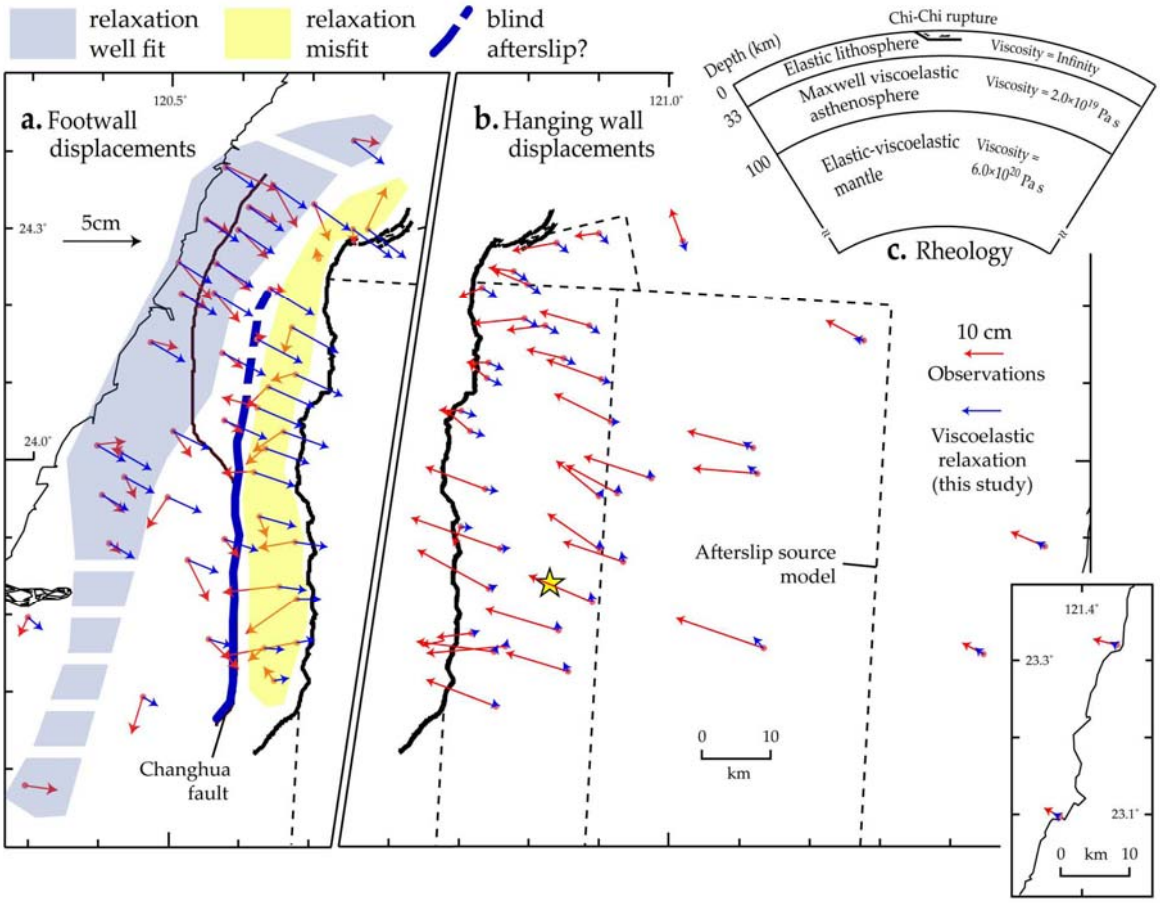

Figure 3. Observed and modelled post-seismic displacements. The footwall (a) and hanging wall (b) vectors are shown separately at different displacement scales. The inset is at the same spatial scale. Relaxation fits the footwall deformation more than 10 km from the fault well, but has no effect on the hanging wall, where the displacements are dominated by afterslip. Post-seismic slip on the southern portion of the Changhua fault is also possible. (c) Rheology used for viscoelastic modelling, based on Johnson *et al.* (2005) and Pollitz (2005).

Although driven by a uniform NW–SE regional tectonic stress (Seno 1977; Hu *et al.* 1996), Taiwan is traversed by high-angle reverse and ramp faults, décollements, and strike-slip faults over a range of depths (Seno 1977; Suppe 1985; Kao & Chen 2000; Chi & Dreger 2004). The diversity of faulting styles is reflected in the focal mechanisms, and for this reason we resolve the Coulomb stress change on several types of 'receiver faults' such as on the nodal planes of focal mechanisms or on fault surfaces in their rake directions.

3 COULOMB STRESS CALCULATIONS

3.1 Stress change for an idealized ramp-décollement model

Because the geometry and slip distribution of the Chi-Chi earthquake are complex, we first illustrate the stress transferred by a simplified Chi-Chi earthquake on an idealized ramp-flat thrust fault system (Fig. 4). While the coseismic slip was greater on the ramp, afterslip is inferred by Yu *et al.* (2003) to be greater on the décollement, and so these distributions are reflected in the idealizations. In addition, most focal mechanisms of the Chi-Chi aftershocks are both thrust and strike-slip, and so the coseismic stress changes are resolved on both types of receiver planes. For 30°-dipping thrust faults (upper panels of Fig. 4), the coseismic slip drops the stress throughout the upper 15 km, or much of the seismogenic depth.

Since much of the background seismicity occurs on north-striking left-lateral faults (Seno 1977; Hu *et al.* 1996; Ma *et al.* 2005), we resolve the stress changes on these receiver planes in the lower panels of Fig. 4. The afterslip tends to re-load parts of the upper crust (Fig. 4j). Unlike the pattern for thrust receivers, the stress transfer to strike-slip receiver faults shows an antisymmetrical distribution, which arises because the rake of the source fault is perpendicular to the rake of the receivers (Figs 4d and i).

3.2 Association of aftershocks with coseismic stress changes

We next calculate the Coulomb stress change using the full Johnson and Segall (2004) coseismic model. Because the majority of the aftershock focal mechanisms are consistent with low-angle thrust slip (Fig. 5a), we use receiver fault

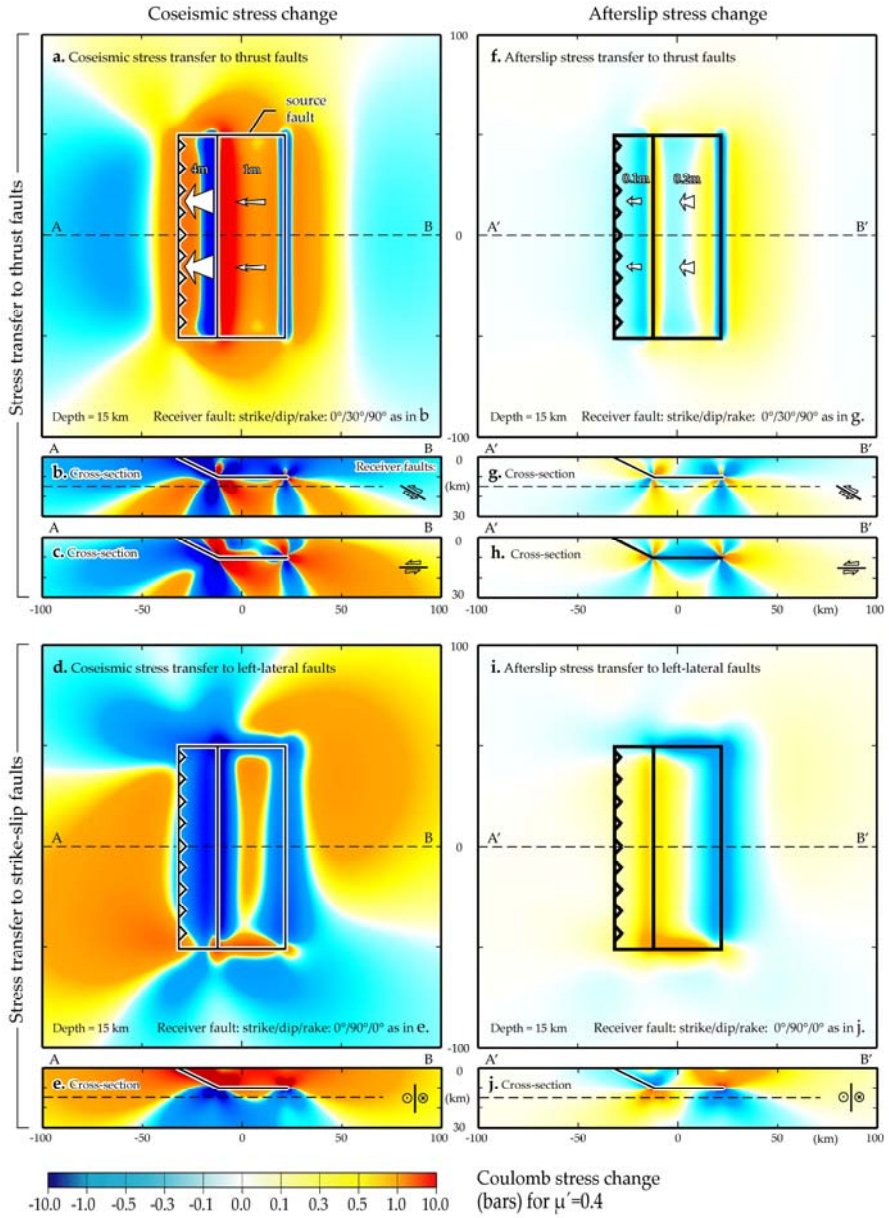

Figure 4. Coulomb stress changes associated with an idealized Chi-Chi ramp-décollement rupture. (a–c) Coseismic stress changes, with higher slip on the ramp segment compared with décollement. The target depth of 15 km corresponds to the average depth of events in the first 3 months after the Chi-Chi earthquake. (d and e) Coseismic stress changes on north-striking left-lateral receiver faults. (f–h) Post-seismic stress changes, with smaller slip on the ramp than the décollement, resolved on thrust faults. (i and j) Post-seismic stress changes resolved on north-striking left-lateral receiver faults.

planes similar to in the idealized Figs 4(a) and (b), consistent with the Chi-Chi main shock: 30°dipping thrust faults striking parallel to the Chelungpu fault with rakes of 80°. The resemblance between the idealized and detailed models is evident (Figs 4a, 5b and c), with the exception that in Figs 5(b) and (c), we show the Coulomb stress change at the specified depths. In Fig. 5, we also use different receiver faults in the two boxed regions dominated by oblique (Pakuashan) and strike-slip (Fengshan) mechanisms. These assignments are based on the identified focal mechanism of the largest aftershock in each region, and the fault plane is distinguished from the nodal plane from seismicity alignments evident in Fig. 5(a). Some 83 per cent of $M > 4$ earthquakes (denoted in the figure by focal mechanisms) lie in regions of Coulomb stress increases of >0.1 bar for the assumed receiver fault orientations indicated in Fig. 5(a). Some 44 per cent of the aftershocks above the décollement (Fig. 5b), 70 per cent of those below (Fig. 5c) and 61 per cent of total lie in regions of calculated >0.1-bar Coulomb stress changes.

To further compare the Coulomb stress change and aftershocks, five cross-sections are presented in Fig. 6 along the routes shown in Figs 5(b) and (c). Here the stress is resolved on the dominant local mechanism, which in most cases is a low-angle thrust fault. Some 74 per cent of the focal mecha-

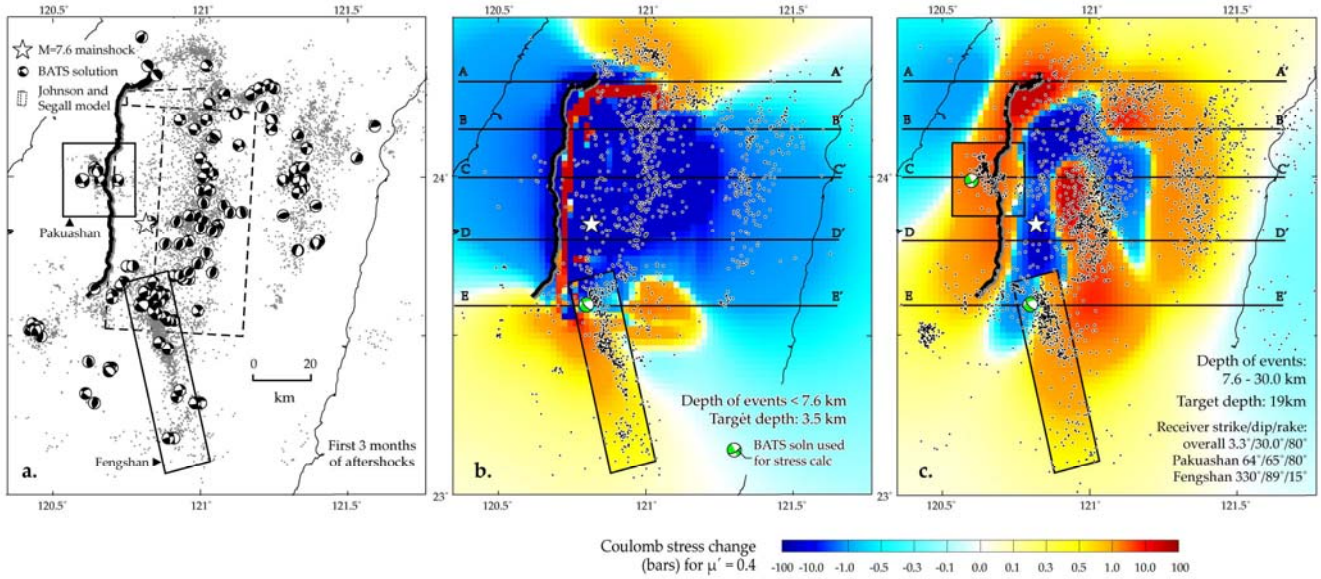

Figure 5. (a) Seismicity and focal mechanisms for the first 3 months after the Chi-Chi earthquake (1999 September–December), using the double-difference algorithm of Waldhauser & Ellsworth (2000). There are 1534 and 2895 $M > 2.0$ events above and beneath the décollement, respectively. The focal mechanisms were acquired by moment tensor inversion of waveforms recorded by the Broadband Array in Taiwan for Seismology (BATS) (Kao *et al.* 2002). The star denotes the epicentre of the Chi-Chi main shock. (b) Coseismic Coulomb stress change on the depth of 3.5 km. (c) Coseismic Coulomb stress change on the depth of 19 km. The black rectangles within green focal mechanisms mark the presumed fault planes on which stress is resolved in the Pakuashan and Fengshan regions. The Coulomb stress increased by >0.1 bar on 82 per cent of the focal planes shown in (a).

nisms of $M > 4$ aftershocks lie in regions of >0.1 bar Coulomb stress increase. Nevertheless, many $M > 2$ aftershocks lie above the décollement, where the Coulomb stress on 30°-dipping thrust faults is calculated to have decreased. These earthquakes would only be consistent with stress transfer if they struck on faults with different orientations, such as horizontal décollements (as shown for the idealized Chi-Chi rupture in Fig. 4c). Because we lack focal mechanisms for most of the $M > 2$ shallow aftershocks, this question is unresolved.

3.3 Stress change on aftershock nodal planes

As an alternative assessment of the efficacy of the stress changes in promoting aftershocks we examine the percentage of aftershock nodal planes with stress increased by the coseismic slip (Fig. 7), following Hardebeck *et al.* (1998). Because of the nodal plane uncertainty for the aftershocks, this calculation is unambiguous only for the shear stress change, or if we assume the friction is very low. What matters in these comparisons is the gain in the percentage of positively stressed mechanisms, which is tallied to the right of the graph, rather than the absolute numbers. We compare the percentage of stress increases on focal mechanisms during the 53-month period before Chi-Chi (the control period) to the period 3–15 months after the Chi-Chi main shock (the test period), and find a 12 per cent gain for aftershocks with shear stress increases >0.1 bars (Fig. 7a), and a 11 ± 3 per cent gain for Coulomb stress increase of >0.1 bars (Fig. 7b). For the Coulomb stress changes, we assume $\mu = 0.4$, and randomly choose one nodal plane of each pair in 10 realizations, and then report the mean and standard deviation. We use the period 3–15 months post-Chi Chi because Ma *et al.* (2005) found that the first 3 months did not show seismicity rate drops in the stress shadows and so might be dominated by dynamic stress or shaking effects, and because post-seismic surveys conducted 15 months after the main shock were used to develop the afterslip model.

Thus this study and its forerunner, Ma *et al.* (2005), demonstrate that even when the source geometry and slip distribution are complex, Coulomb stress transfer is correlated with the distribution of aftershocks and their focal mechanisms. The next question we tackle is whether the stresses also govern the afterslip.

3.4 Coseismic stress change resolved on the post-seismic surface

To understand the influence of coseismic stress change on afterslip, we calculate the stress imparted by the coseismic slip of the Johnson and Segall (2004) (Fig. 8) on the ramp and décollement. This calculation would be straightforward if the afterslip occurred exclusively off the coseismic rupture, such as on its downdip or along-strike extensions. However parts of the coseismic slip surface are inferred by Yu *et al.* (2003) to have slipped further during the post-seismic period, and the coseismic slip discontinuities cause large local stress changes on the fault. We thus smoothed the stress changes with a Gaussian nearest-neighbour filter, iterated as specified in Table 1. Johnson & Segall (2004) use an 8-km depth for the décollement, whereas Yu *et al.* (2003) use 10 km. The difference is beyond the resolution of the geodetic data, and so we calculate stress changes within a layer extending from 3 km

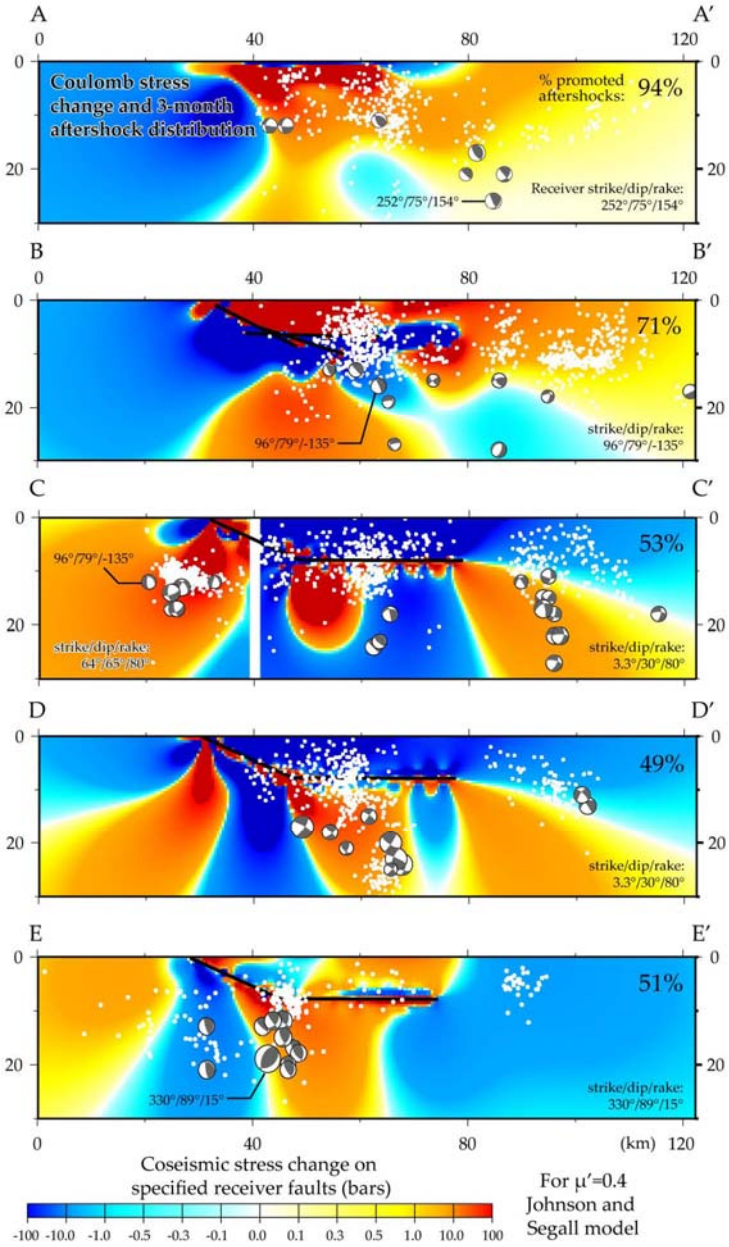

Figure 6. Five cross-sections of the Coulomb stress change associated with the first 3 months of aftershocks and focal mechanisms within 5 km of each profile marked on Fig. 5. Black lines denote the coseismic rupture fault geometry based on Johnson & Segall (2004). The strike/dip/rake of 3.3°/30°/80° is the Chi-Chi main shock mechanism; other receiver fault orientations are based on the indicated focal mechanisms and the associated seismicity alignments in each panel. Section AA lies north of the fault plane, amid strike-slip mechanisms aligned N80' W. In CC, stress is resolved on the two receiver faults that correspond the local focal mechanisms, with a white vertical band dividing this composite section. The percentage of aftershocks in the >0.1-bar Coulomb stress change regions is given in the upper right of each panel.

above to 3 km below the ramp and décollement. In other words, at every horizontal position, we report the average stress change calculated over a depth range within 3 km of the fault; this diminishes the importance of the uncertainty in the depth of the décollement. The resulting stress changes are still far from smooth, making comparisons of coseismic stress to afterslip qualitative.

The coseismic slip causes a shear stress increase downdip of the hypocentre, and a shear stress decrease on the upper 5 km of the ramp (Fig. 8b). Afterslip apparently extends nearly to the ground surface, where the coseismic slip is calculated to cause unclamping and a shear stress decrease (Figs 8b and c). We find a positive correlation between coseismic shear stress increase and post-seismic slip on 60 per cent of the décollement surface; a positive correlation is found between coseismic unclamping and post-seismic slip on 67 per cent of the ramp surface.

The Coulomb stress changes imparted by the coseismic slip could thus have at least partly driven the afterslip if the effective friction on the décollement surface, μ', were very

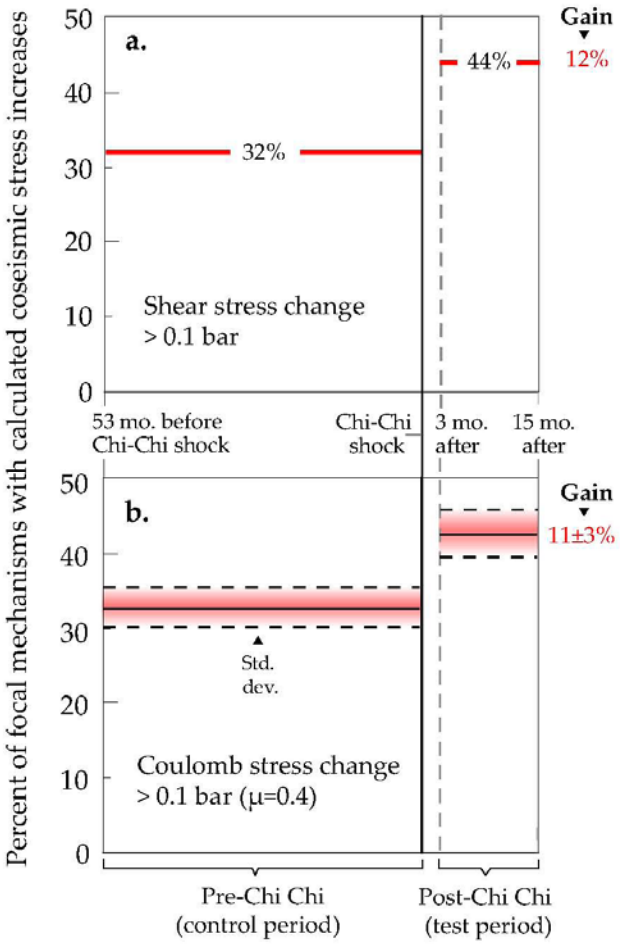

Figure 7. Increase in the percentage of focal mechanisms with (a) shear stress increases and (b) Coulomb stress increase >0.1 bar imparted by the coseismic slip.

low. Independent evidence suggests that because décollement surfaces are not optimally aligned in a compressive tectonic regime, they can only slip if they possess very low friction, caused either by layer interbeds, extensive gouge zones, or high-pore fluid pressure (Barr & Dahlen 1989; Byrne & Fisher 1990), and so this inference may be reasonable.

3.5 Post-seismic stress change associated with post-seismic seismicity

Next we seek to understand whether stress changes induced by the afterslip and post-seismic deformation alter the seismicity rate and its distribution. In other words, to what extent is the aftershock sequence anomalous once afterslip and viscoelastic relaxation have progressed. To isolate aftershocks with a decaying frequency from the presumably more steady background seismicity, we create a projected aftershock rate map using earthquakes above the magnitude of completeness, M_c. For the 50-month pre- and post-Chi Chi periods, $M_c < 2$ in the interior of Taiwan; $M_c < 3$ for regions within about 100 km of the coastline (Ma *et al.* 2005). To capture a sufficient

Table 1. The number of smoothing passes specified on each fault surface in Fig. 8. Every point is averaged with the value of its eight neighbours iteratively.

Coseismic shear stress change		Coseismic unclaming stress change	
Ramp	Décollement	Ramp	Décollement
5	20	5	10

number of earthquakes with these magnitudes, we use 50 km x 50 km cells.

We first subtract the 50-month pre-Chi Chi seismicity rate from the rate observed during the first 3 months of aftershocks to remove the steady background seismicity. This step is important for sites far from the Chi-Chi main shock where the background rate is high and there are few aftershocks. We then fit the decay in each cell to the 3–15 month residuals, using modified Omori's law (Utsu 1961), solving for the decay exponent p, which is generally found to be about 1.0, and for the c term in $n(t) = k/(c + t)^{-p}$, where n is the number of aftershocks in a cell. A representative time series for one cell is shown in Fig. 9(a). In Fig. 10, we plot the seismicity rate change, the ratio of the rate 15–53 months to 3–15 months after the Chi-Chi earthquake. The resulting p values are given for each cell. Because we are taking a ratio of late to early aftershock rates, the productivity term k falls out; since c is thought to originate from catalogue incompleteness immediately after the main shock, we do not report it here. Sites with $p \sim 1$, which extend up to 100 km from the fault, experienced a rapid decay of aftershock frequency during the first 3 months. Sites with $p \sim 0$ exhibited steady seismicity rates with no discernable aftershocks.

The observed late aftershock sequence is shown in Fig. 10(b); this is simply the observed ratio of the rate 15–53 to 3–15 months after the Chi-Chi main shock. The distribution shows a broad seismicity rate drop in central Taiwan region centred on the Chi-Chi décollement, consistent with aftershock decay during the first 15 months (Fig. 10a). However, there is a semi-annulus of seismicity rate increases extending east of the main shock labelled 'E. offshore annulus' in Fig. 10(b), as well as a cell 50 km north of the northern end of the fault rupture which also experienced a seismicity rate increase. Only 3–4 of the 12 cells with observed increases are associated with $M > 6$ shocks that occurred 15–53 months after the main shock. In contrast to the aftershock decay near the fault rupture, the time series in the East offshore annulus 100–200 km from the main shock (Fig. 10b), exhibits no decay during the post-seismic period (Fig. 9b). Instead, an increase in seismicity rate is observed from 2000 onward, punctuated by several $M > 6$ shocks in 2002–2004. During the first 3 months, six out of the seven measurable cells in the E. offshore annulus exhibited rate decays, whereas all show rate increases afterwards. Further, even annulus cells several hundred kilometres from the $M \geq 6$ shocks show rate increases. Thus, we argue that this broad annulus of seismicity rate increase is associated with the post-seismic stressing.

The observed departure from Omori decay resembles the calculated stresses imparted by afterslip and relaxation in Figs 10(c) and (d), particularly for regions off the main fault rupture. The East offshore annulus is expected to be the site of

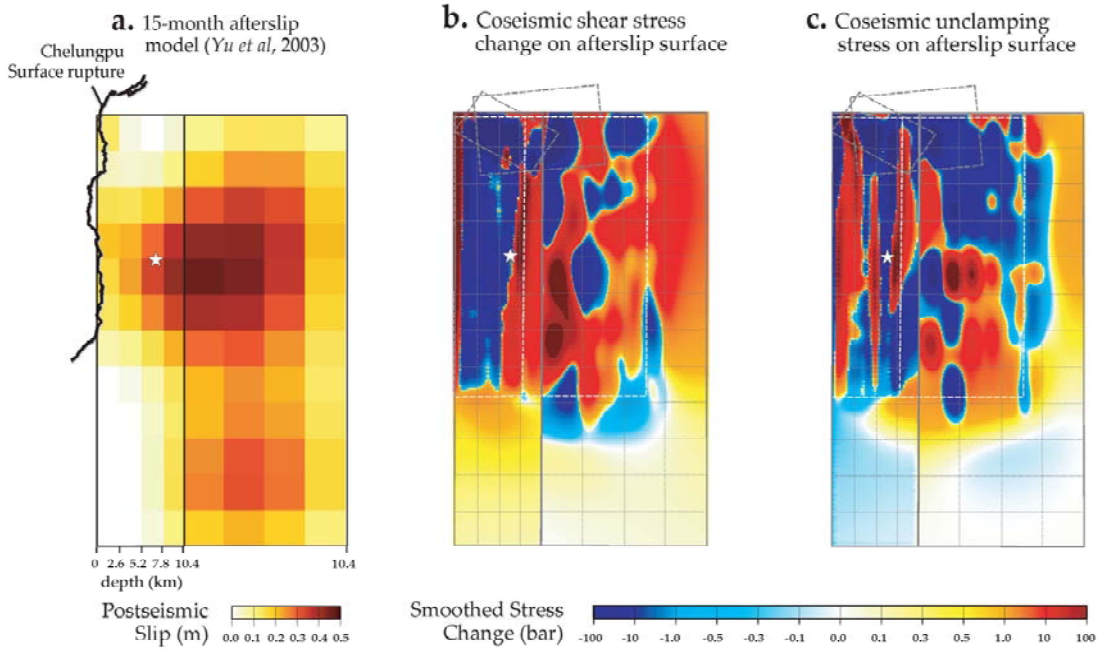

Figure 8. (a) Afterslip model of Yu *et al.* (2003). Shear (b) and unclamping (c) stress imparted by the coseismic slip resolved on the afterslip surfaces. In order to eliminate the stress discontinuities on the source rupture, the data are iteratively smoothed by averaging each point with its eight neighbours, as specified in Table 1.

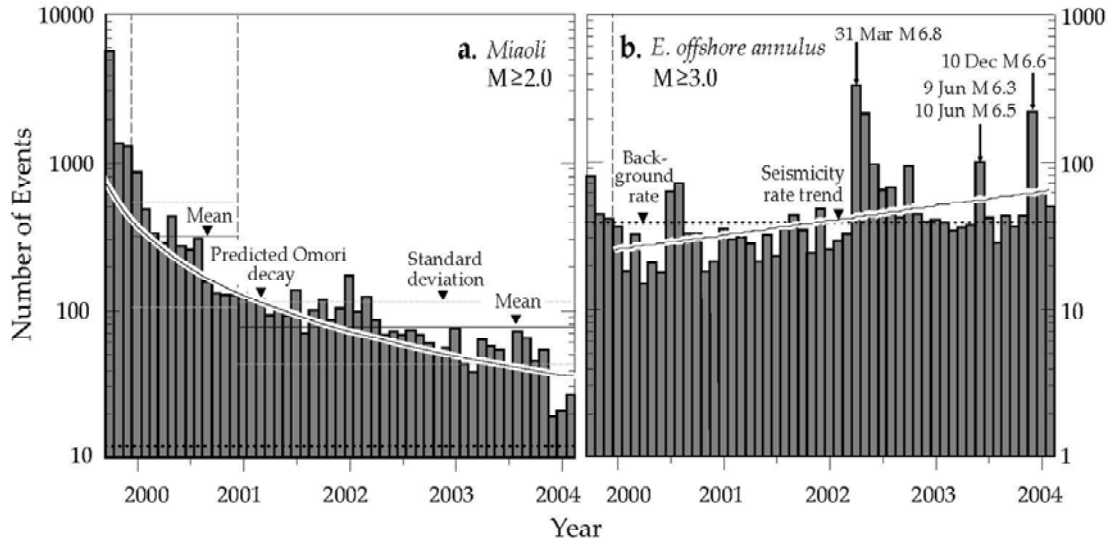

Figure 9. Time series of seismicity beginning 3 months after the Chi-Chi main shock for (a) Miaoli and (b) the East offshore annulus inscribed in Fig. 10(b).

thrust earthquakes, and both thrust and strike-slip faults should experience stress increases both northeast and north of the rupture, in accord with the observed seismicity rate increases (Fig. 10b) and observed focal mechanisms (Figs 10c and d). The target depth of 20 km used in Figs 10(c) and (d) is consistent with the average depth of earthquake hypocentres. The depth and focal mechanism-dependence of these patterns can be judged from idealized cross-sections of Figs 4(g) and (j). The offshore seismicity increase was accompanied by four $M \geq 6$ shocks; these shocks could have been promoted by the stress increase, and they undoubtedly contribute to the seismicity rate increase. The decrease in Coulomb stress over the décollement is also evident in Figs 10(c) and (d).

There is fair correspondence between the calculated postseismic Coulomb stress changes with focal mechanisms in Figs 10(c) and (d), with 59 per cent of the strike-slip mechanisms and 73 per cent of the thrust mechanisms after 2000 December occurring in regions of expected Coulomb increase. Further, the Coulomb stress change on strike-slip faults is increased in 54 per cent of the area in East offshore

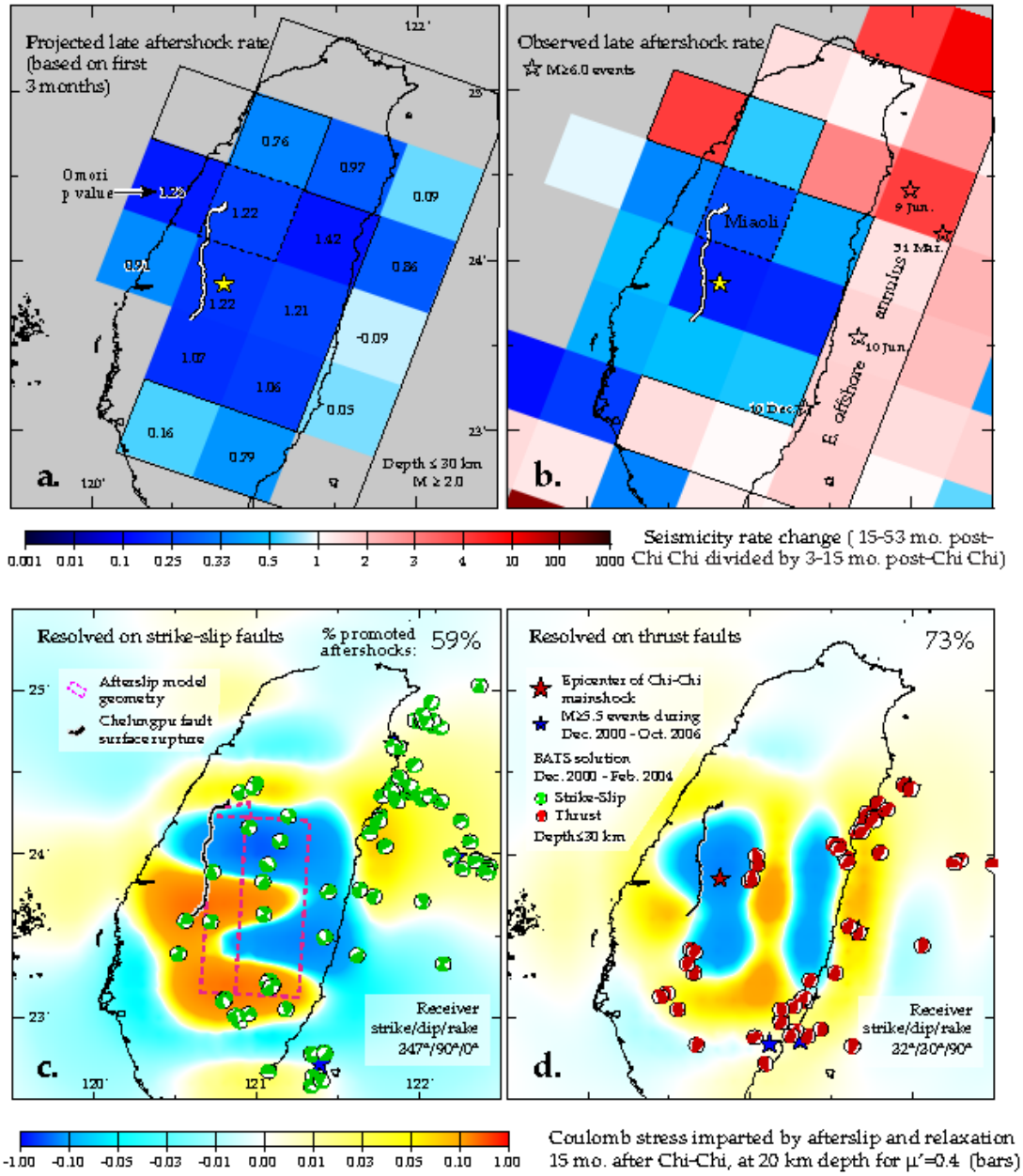

Figure 10. (a) Projected aftershock rate based on the first 3-month decay. The measured *p*-value of Omori decay for each grid is shown. (b) Observed seismicity rate change, beginning 15 months after the Chi-Chi earthquake. The cells are 50 x 50 x 30 km for $M \geq 2$ earthquakes; this area is needed to contain a sufficient number of earthquakes to solve for *p*. (c and d) Coulomb stress changes caused by viscoelastic deformation and afterslip 15 months after Chi-Chi resolved on to northwest-striking left-lateral (c) and northeast-striking thrust (d) faults at 20 km depth. The Coulomb stress at 53 months has the same distribution but is about 15 per cent higher.

annulus by post-seismic processes, and 76 per cent of the annulus is enhanced for thrust faults. Table 2 gives the shear stress change on the $M \geq 5.5$ mechanisms that took place after the first 15 months; since the fault plane cannot be distinguished from the nodal plane, the unclamping stress is ambiguous and so the Coulomb stress is uncertain. About 57 per cent of these events are calculated to have sustained coseismic+post-seismic shear stress increases.

We also tested the percent of aftershock focal mechanisms with shear stress increases imparted by the afterslip and relaxation, and find increases of 9–12 per cent over the pre-Chi Chi control period (Fig. 11). In Fig. 11, it is also evident that the percentage of encouraged mechanisms increases with time following the main shock, as would be expected since afterslip and relaxation occur over a period longer than 15 months. In contrast, the percentage of mechanisms encouraged by the coseismic stresses drops by 4–10 per cent after the first 15 months, reinforcing our inference that the stresses evolve over time. For the Coulomb stress the increase is not significant (3 ± 3 per cent) perhaps because of the nodal plane ambiguity,

Table 2. The shear stress change resolved on the nodal planes of the $M \geq 5.5$ aftershocks that struck during the period 15–53 months after the Chi-Chi main shock. Some 57 per cent of shocks are associated with net coseismic plus post-seismic shear stress increases, and 86 per cent are associated with post-seismic shear stress increases alone. The unclamping stress cannot be determined with confidence because of nodal plane ambiguity. The focal mechanisms were acquired by moment tensor inversion of waveforms recorded by the Broadband Array in Taiwan for Seismology (BATS) (Liang *et al.* 2003, 2004).

No.	Time (yr/month/d)	Latitude (°)	Longitude (°)	Depth (km)	Strike (°)	Dip (°)	Rake (°)	Coseis. $\Delta\sigma_s$ (bars)	Postesis. $\Delta\sigma_s$ (bars)
1	2001/06/14	24.42	121.93	28	85	48	-25	-0.219	-0.077
2	2001/12/18	23.87	122.65	12	231	56	-9	0.119	0.033
3	2002/05/15	24.65	121.87	17	20	49	167	-0.033	0.006
4	2002/05/28	23.91	122.40	27	312	37	154	0.037	0.077
5	2003/06/09	24.40	121.99	22	225	26	121	-0.027	-0.043
6	2003/06/10	23.52	121.67	29	9	47	66	-0.321	0.065
7	2003/12/10	23.10	121.34	20	23	42	104	-0.058	0.186
8	2004/05/08	21.96	121.49	24	178	28	100	0.011	0.003
9	2004/05/19	22.70	121.39	19	338	39	20	0.093	0.033
10	2004/11/08	23.85	122.58	21	359	30	-140	0.047	0.291
11	2005/03/05	24.67	121.85	19	270	66	-10	-0.107	0.019
12	2005/09/06	23.97	122.23	27	329	34	162	0.027	0.065
13	2006/04/01	22.83	121.12	22	92	70	165	-0.070	0.026
14	2006/04/15	22.85	121.31	18	348	45	52	0.089	0.044

or because fault friction is lower than the tested value of 0.4 (Fig. 11b).

4 DISCUSSION AND CONCLUSIONS

4.1 Coseismic and post-seismic slip in crustal unloading and reloading

Stress is imparted to the crust surrounding the Chelungpu fault from three sources: the coseismic slip, aftershocks, and post-seismic processes including afterslip and relaxation. The relative magnitudes of these sources can be gauged in Fig. 12, which makes clear that afterslip alone contributes more seismic moment than aftershocks. Afterslip carries 3.5 the moment of the largest ($M \geq 6$) aftershocks. Including $M \geq 4$ shocks increases the moment of the aftershocks by 15 per cent, to 1.7 x 10^{19} Nm. For a *b*-value near 1, afterslip contributes about 2.5 times the moment of all aftershocks.

The Coulomb stress imparted by slip on a ramp-décollement system is quite unlike that of a continental blind thrust fault (Lin & Stein 2004) or subduction megathrust (Hsu *et al.* 2006) because the upper crust (<8–10 km depth) is brought farther from failure while the crust beneath the décollement is brought closer to failure (Fig. 4b). Afterslip on the décollement acts to reload the upper crust (Fig. 4g). In contrast, blind thrust faults without décollements tend to increase the failure stress in the upper crust coseismically, producing diffuse and highly productive aftershock sequences (Lin & Stein 2004).

4.2 Role of coseismic slip in controlling aftershocks

Extending the study of Ma *et al.* (2005), we find that the coseismic Coulomb stress changes are correlated with the distribution of aftershocks both in map view (Fig. 5) and cross-section (Fig. 6). The analysis is complicated by the diversity of focal mechanisms and faulting regimes, but when we resolve stresses on planes corresponding to the principal focal mechanisms in each region, the association of seismicity and calculated Coulomb stress change is evident with correlation coefficients spanning 49–94 per cent. Calculating the stress imparted to aftershock nodal planes, we find that the percentage of focal mechanisms for which the Coulomb stress increased by >0.1 bar as a result of the main shock rose by 11 ± 3 per cent over a control period before the main shock (Fig. 7b).

4.3 Co-location of afterslip with décollement seismicity

As reported by Yu *et al.* (2003), afterslip extends downdip from the peak coseismic slip, covering a larger area of the décollement. During the period of measured afterslip, aftershocks are concentrated where the afterslip is high (Fig. 1b). This zone of seismicity is also at the periphery of the coseismic slip (Fig. 5a), and so it is not clear whether aftershocks occur where the stress imparted by the coseismic slip is high, or where the afterslip is high, or both.

4.4 Role of low décollement friction in promoting afterslip

We argue that the coseismic stress changes drive the occurrence of afterslip. While we have used an intermediate value for the fault friction of $\mu' = 0.4$ for the stress resolved on nodal planes of $M \geq 4$ focal mechanisms, we find that slip on the décollement and the base of the ramp is best correlated with the shear stress change, implying $\mu' \sim 0.0$ (Fig. 8). Thus because a horizontal surface must be profoundly weak to slip, the décollement may exhibit unique properties in comparison to the surrounding crust.

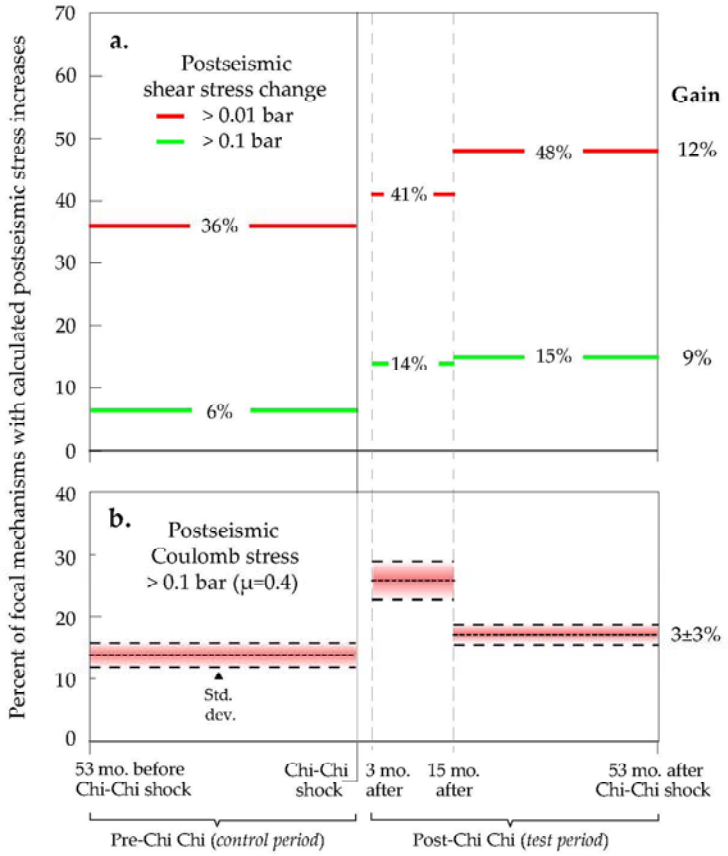

Figure 11. Increase in the percentage of focal mechanisms with (a) shear stress increases and (b) Coulomb stress increase >0.1 (green lines) and > 0.01 (red lines) bar imparted by the afterslip and relaxation.

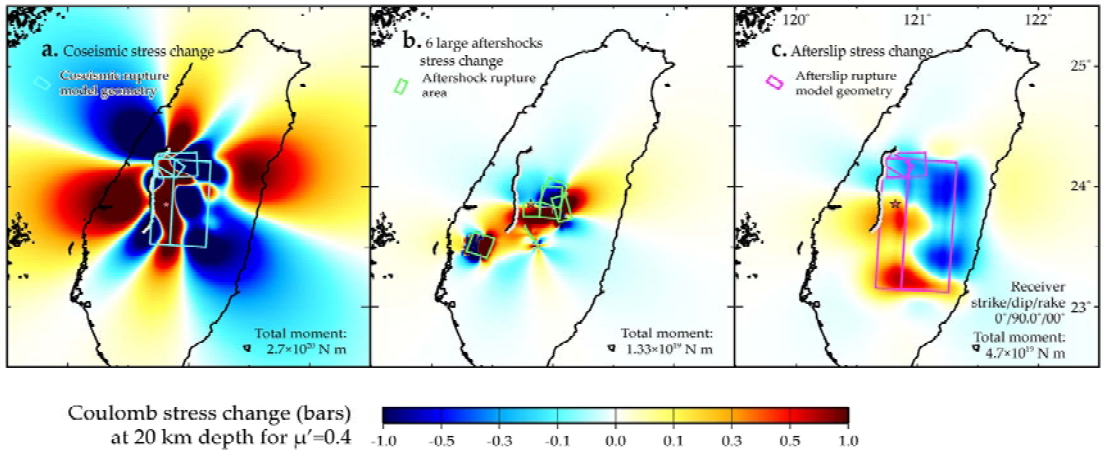

Figure 12. Coulomb stress changes and the total seismic moment imparted by (a) the modelled Chi-Chi coseismic slip, (b) the six $M \geq 6.0$ aftershocks occurring during the first 3 months of the main shock, and (c) the modelled afterslip during the 15-month post-seismic period.

4.5 Simultaneous and viscoelastic deformation processes

Departing from Yu *et al.* (2003), we argue that the post-seismic GPS displacements on the footwall are systematically misfit by afterslip alone. When viscoelastic relaxation is also included, the footwall residuals are greatly reduced (Fig. 3), and the hangingwall residuals are little affected. Relaxation is not confined to the footwall; rather, over the décollement surface GPS displacements from afterslip dwarf displacements associated with relaxation. In subduction zones, the footwall is under water and so its deformation is never measured, rendering the most distinctive signal of relaxation unobtainable for most megathrust earthquakes.

4.6 Aftershock decay departs from the initial distribution following afterslip and relaxation

After most of the measured afterslip had taken place, the observed aftershock rates departed from that projected from the initial 3 months of decay. The seismicity rate in the E. offshore annulus increased, incompatible with - or unrelated to - Omori decay (Fig. 10b). The observed increases correspond spatially to the stresses imparted by afterslip and relaxation (Figs 10c and d), and the percentage of focal mechanisms brought closer to failure by the afterslip and relaxation rose by 9–12 per cent over a control period before the main shock (Fig. 11). The $M \geq 4$ aftershocks beginning 15 months after the Chi-Chi main shock are correlated with the calculated Coulomb stress changes imparted by viscoelastic relaxation and afterslip at the level of 59–73 per cent (Fig. 10c–d).

ACKNOWLEDGMENTS

We thank Fred Pollitz for guidance in the use and interpretation of VISCO1D, Shinji Toda for providing Coulomb 3.1, and Jeanne Hardebeck, Kuo-Fong Ma, Volkan Sevilgen, Massimo Cocco, Rodolfo Console, and Sandy Steacy for thoughtful reviews. We thank the National Science Council of Taiwan for a C.-H. C.'s Fellowship to spend a year at the USGS.

REFERENCES

Barr, T.D. & Dahlen, F.A., 1989. Brittle frictional mountain building, 2. Thermal structure and heat budget, *J. geophys. Res.*, **94**, 3923–3947.

Beeler, N., Simpson, R., Hickman, S. & Lockner, D., 2000. Pore fluid pressure, apparent friction, and Coulomb failure, *J. geophys. Res.*, **105**, 25 533–25 542.

Byrne, T. & Fisher, D., 1990. Evidence for a weak and overpressured décollement beneath sediment dominated accretionary prisms, *J. geophys. Res.*, **95**, 9081–9097.

Chang, C.- H., Wu, Y.-M., Shin, T.-C. & Wang, C.-Y., 2000. Relocation of the 1999 Chi-Chi earthquake in Taiwan, *Terr. Atmos. Oceanic Sci.*, **11**(3), 581–590.

Chi, W.-C., & Dreger, D., 2004. Crustal deformation in Taiwan: Results from finite source inversions of six $M_W > 5.8$ Chi-Chi aftershocks, *J. geophys. Res.*, **109**, B07305, doi:10.1029/ 2003JB002606.

Chi, W.-C., Dreger, D. & Kaverina, A., 2001. Finite-source modeling of the 1999 Taiwan (Chi-Chi) earthquake derived from a dense strong motion network, *Bull. seism. Soc. Am.*, **91**, 1144–1157.

Cocco, M. & Rice, J., 2002. Pore pressure and poroelasticity effects in Coulomb stress analysis of earthquake interactions, *J. geophys. Res.*, **107**, doi:10.1029/2000JB000138.

Freed, A.M., 2005. Earthquake triggering by static, dynamic, and postseismic stress transfer, *Annu. Rev. Earth planet. Sci.*, **2005**(33), 335–67, doi: 10.1146/annurev.earth.33.092203.122505.

Freed, A.M., Ali, S.T. & Bürgmann, R., 2007. Evolution of stress in Southern California for the past 200 years from coseismic, postseismic and interseismic stress changes, *Geophys. J. Int.*, **169**, 1164–1179 doi:10.1111/j.1365-246X.2007.03391.x.

Hardebeck, J.L., Nazareth, J.J. & Hauksson, E., 1998. The static stress change triggering model: constraints from two southern California aftershocks sequences, *J. geophys. Res.*, **103**, 24 427– 24 437.

Harris, R.A., 1998. Introduction to special section: stress triggers, stress shadows, and implications for seismic hazard, *J. geophys. Res.*, **103**, 24 347–24 358.

Hsu, Y.-J., 2004. Modeling studies on interseismic, coseismic and postseismic deformations associated with the 1999 Chi-Chi, Taiwan earthquake, *Ph.D. dissertation*. 112 pp., Natl. Cent. Univ., Taiwan.

Hsu, Y.-J., Simons, M., Avouac, J.P., Galetzka, J., Sieh, K., Chlieh, M., Natawidjaja, D., Prawirodirdjo, L. & Brock, Y., 2006. Frictional afterslip following the 2005 Nias-Simeulue earthquake, Sumatra, *Science*, **312**(5782), 1921–1926.

Hu, J.-C., Angelier, J., Lee, J.-C., Chu, H.-T. & Byrne, D., 1996. Kinematics of convergence, deformation and stress distribution in the Taiwan collision area: 2-D Finite-element numerical modeling, *Tectonophysics*, **255**, 243–268.

Ji, C., Helmberger, D.V., Wald, D.J. & Ma, K.-F., 2003. Slip history and dynamic implications of the 1999 Chi-Chi, Taiwan, earthquake, *J. geophys. Res.*, **108**, 2412, doi:10.1029/2002JB001764.

Johnson, K.M. & Segall, P., 2004. Imaging the ramp–décollement geometry of the Chelungpu fault using co-seismic GPS displacements from the 1999 Chi-Chi, Taiwan earthquake, *Tectonophys.*, **378**, 123–139.

Johnson, K.M., Segall, P. & Yu, S.B., 2005. A viscoelastic earthquake cycle model for Taiwan, *J. geophys. Res.*, **110**, doi:10.1029/2004JB003516.

Kao, H. & Chen, W.-P., 2000. The Chi-Chi earthquake sequence: active, out-of-sequence thrust faulting in Taiwan, *Science*, **288**, 2346– 2349.

Kao, H., Liu, Y.-H., Liang, W.-T. & Chen, W.-P., 2002. Source parameters of regional earthquakes in Taiwan: 1999–2000 including the Chi-Chi earthquake sequence, *Terr. Atmos. Oceanic Sci.*, **13**, 279– 298.

King, G.C.P. & Cocco, M., 2000. Fault interaction by elastic stress changes: new clues from earthquake sequences, *Adv. Geophys.*, **44**, 1–36.

King, G.C.P., Stein, R.S. & Lin, J., 1994. Static stress changes and the triggering of earthquakes, *Bull. seism. Soc. Am.*, **84**, 935–953.

Liang, W.-T., Liu, Y.-H. & Kao, H., 2003. Source parameters of regional earthquakes in Taiwan: January-December 2001, *Terr., Atmos. Ocean Sci.*, **14**, 249–260.

Liang, W.-T., Liu, Y.-H. & Kao, H., 2004. Source parameters of regional earthquakes in Taiwan: January-December 2002, *Terr., Atmos. Ocean. Sci.*, **15**, 727–741.

Lin, J. & Stein, R.S., 2004. Stress triggering in thrust and subduction earthquakes, and stress interaction between the

southern San Andreas and nearby thrust and strike-slip faults, *J. geophys. Res.*, **109**, B02303, doi:10.1029/2003JB002607.

Ma, K.-F., Lee, C.T., Tsai, Y.B., Shin, T.C. & Mori, J., 1999. The 1999 Chi-Chi, Taiwan (M_L = 7.3, M_w = 7.7) earthquake—large surface displacement on an Inland thrust-fault, *EOS*, **80**, 605–611.

Ma, K.-F., Mori, J., Lee, S.-J. & Yu, S.-B., 2001. Spatial and temporal distribution of slip for the 1999 Chi-Chi, Taiwan earthquake, *Bull. seism. Soc. Am.*, **91**, 1–19.

Ma, K.-F., Chan, C.-H. & Stein, R.S., 2005. Response of seismicity to Coulomb stress triggers and shadows of the 1999 M_w = 7.6 Chi-Chi, Taiwan, earthquake, *J. geophys. Res.*, **110**, doi:10.1029/2004JB003389.

Parsons, T., 2002. Global observation of Omori-law decay in the rate of triggered earthquakes: large aftershocks outside the classical aftershock zone, *J. geophys. Res.*, **107**, 2199, doi:10.1029/2001JB0006462.

Parsons, T., Stein, R.S., Simpson, R.W. & Reasenberg, P.A., 1999. Stress sensitivity of fault seismicity: a comparison between limited-offset oblique and major strike-slip faults, *J. geophys. Res.*, **104**, 20 183–20 202.

Perfettini, H. & Avouac, J.-P., 2004. Postseismic relaxation driven by brittle creep: a possible mechanism to reconcile geodetic measurements and the decay rate of aftershocks, application to the Chi-Chi earthquake, Taiwan, *J. geophys. Res.*, **109**, B02304, doi:10.1029/2003JB002488.

Pollitz, F.F., 2005. Transient rheology of the upper mantle beneath central Alaska inferred from the crustal velocity field following the 2002 Denali earthquake, *J. geophys. Res.*, **110**, B08407, doi:10.1029/2005JB003672.

Pollitz, F.F., Bakun, W.H. & Nyst, M., 2004. A physical model for strain accumulation in the San Francisco Bay region: stress evolution since 1838, *J. geophys. Res.*, **109**, B11408, doi:10.1029/2004JB003003.

Pollitz, F.F., Nyst, M., Nishimura, T. & Thatcher, W., 2006. Inference of postseismic deformation mechanisms of the 1923 Kanto earthquake, *J. geophys. Res.*, **111**, doi:10.1029/2005JB003901.

Rundle, J.B. & Jackson, D.D., 1977. A kinematic viscoelastic model of the San Francisco earthquake of 1906, *Geophys. J. R. astron. Soc.*, **50**, 441–458.

Savage, J.C., 1990. Equivalent strike-slip earthquake cycles in half-space and lithosphere-asthenosphere Earth models, *J. geophys. Res.*, **95**, 4873– 4879.

Seno, T., 1977. The instantaneous rotation vector of the Philippine Sea Plate relative to the Eurasian Plate, *Tectonophysics*, **42**, 209–226.

Sheu, S.-Y. & Shieh, C.-F., 2004. Viscoelastic-afterslip concurrence: a possible mechanism in the early post-seismic deformation of the M_w 7.6 1999 Chi-Chi (Taiwan) earthquake, *Geophys. J. Int.*, **159**, 1112–1124, doi:10.1111/j.1365-246X.2004.02437.x.

Steacy, S., Gomberg, J. & Cocco, M., 2005. Introduction to special section: stress transfer, earthquake triggering, and time-dependent seismic hazard, *J. geophys. Res.*, **110**, B05S01, doi:10.1029/2005JB003692.

Stein, R.S., 1999. The role of stress transfer in earthquake occurrence, *Nature*, **402**, 605–609.

Suppe, J., 1985. *Principles of Structural Geology*, pp. 537, Prentice-Hall, Englewood Cliffs.

Thatcher, W., 1983. Nonlinear strain build-up and the earthquake cycle on the San Andreas fault, *J. geophys. Res.*, **88**, 5893–5902.

Toda, S. & Stein, R.S., 2002. Response of the San Andreas Fault to the 1983 Coalinga-Nuñez Earthquakes: An Application of Interaction-based Probabilities for Parkfield, *J. geophys. Res.*, **107**, doi:10.1029/2001JB000172.

Toda, S., Stein, R.S., Reasenberg, P.A., Dieterich, J.H. & Yoshida, A., 1998. Stress transferred by the M_w = 6.9 Kobe, Japan, shock: effect on aftershocks and future earthquake probabilities, *J. geophys. Res.*, **103**, 24 543–245 65.

Utsu, T., 1961. A statistical study on the occurrence of aftershocks, *Geophys. Mag.*, **30**(4), 521–605.

Waldhauser, F. & Ellsworth, W.L., 2000. A double-difference earthquake location algorithm: method and application to the northern Hayward fault, *Bull. seism. Soc. Am.*, **90**, 1353–1368.

Yu, S.B. *et al.*, 2001. Preseismic deformation and coseismic displacements associated with the 1999 Chi-Chi, Taiwan earthquake, *Bull. seism. Soc. Am.*, **91**, 995–1012.

Yu, S.-B., Hsu, Y.-J., Kuo, L.-C. & Chen, H.-Y., 2003 GPS measurement of postseismic deformation following the 1999 Chi-Chi, Taiwan, earthquake, *J. geophys. Res.*, **108**, 2412, doi:10.1029/2003JB002396.

Yue, L.-F., Suppe, J. & Hung, J.-H., 2005. Structural geology of a classic thrust belt earthquake: the 1999 Chi-Chi earthquake Taiwan (M_w = 7.6), *J. Struct. Geol.*, **27**, 2058–2083.

Zeng, Y.H. & Chen, C.H., 2001. Fault rupture process of the 20 September 1999 Chi-Chi, Taiwan, earthquake, *Bull. seism. Soc. Am.*, **91** 1088–1098.

Zoback, M.D. *et al.*, 1987. New evidence on the state of stress of the San Andreas Fault system, *Science*, **238**, 1105–1111.